

Experimental study and Large Eddy Simulation of Laser Ignition in a Rocket Like Configuration

G. Lacaze¹, B. Cuenot¹, T. Poinsot² and M. Oswald³

February 20, 2008

¹ CERFACS, 42 Avenue G. Coriolis, 31057 Toulouse cedex, France

² Institut de Mécanique des Fluides de Toulouse, CNRS, Avenue C. Soula, 31400 Toulouse, France

³ DLR Lampoldshausen, 74239 Hardthausen, Germany

Corresponding author:

G. Lacaze

CERFACS - 42 Avenue Coriolis

31057 TOULOUSE CEDEX FRANCE

FAX: 33 5 61 19 30 00 - EMAIL: lacaze@cerfacs.fr

Colloquium: 13.

Short title: Large Eddy Simulation of Laser ignition

Total length of paper: 5779 words

Listing of word count: Main text (3343) Equations (194) References (671) Figures (1571)

Abstract

The Control of the ignition sequence in a rocket engine is a critical problem for present and future combustion chamber designs. In some cases delayed ignition may lead to a chamber pressure peak that could damage the burner. This paper describes a joint numerical and experimental study of a violent ignition sequence in a laboratory-scale H₂-O₂ rocket chamber ignited by a laser. Schlieren views and pressure measurements allow to follow the flame propagation experimentally. The LES includes shock capturing, a 6 species - 7 reactions for H₂-O₂ and a new model for energy deposition by a laser. The flame/turbulence interaction model is the thickened flame model. LES is used to compute the filling phase (where the chamber is filled with gaseous hydrogen and oxygen) and the ignition phase. The flame positions observed experimentally and numerically agree as well as the pressure curves in the chamber. The LES has shown that the delayed ignition leads to a long filling phase during which hydrogen and oxygen mix into the chamber. When ignition occurs the flame propagates rapidly in a partially-premixed combustion mode implying a sharp pressure peak in the vessel.

Keywords:

IGNITION, NUMERICAL COMBUSTION, ROCKET ENGINES

1. Introduction

Large Eddy Simulation (LES) is a powerful tool to study unsteady complex flows. The concept of explicitly solving for the large geometry-dependent turbulent scales while modelling the dissipative behavior of the smaller scales, combined with high order numerical schemes and optimized unstructured meshes, has already shown its accuracy for turbulent non-reacting [1–3] and reacting flows [4–6] and recent results obtained on burners of gas turbine configurations are very encouraging [7–10]. The application of LES to unsteady combustion in rocket engines is even more recent and faces specific problems such as high compressibility (including shocks) and very fast chemical reactions [11].

The present paper is a first step towards the application of LES to ignition in rocket engines. The ignition sequence, the compressible nature of the flow (with supersonic inlets) and the fast H₂-O₂ chemistry require a specific methodology developed herein. The validation is performed on the experiment of DLR [12] that reproduces laser ignition in rocket engine-like conditions.

Previous modeling works of Schmidt et al [13] and Karl et al [14] have been carried out on this configuration. The numerical work presented in [13] is preliminary research using a Reynolds-Averaged Navier-Stokes method (RANS) and the ignition transient was not completed. The RANS simulation carried out by Karl et al [14] overestimated the pressure peak. Several explanations were formulated : nitrogen dilution was neglected as well as turbulent effects, the geometry was simplified and no heat loss was considered. Section 2 describes the physics of ignition in rocket engines and section 3 presents the ignition experiment. Section 4 develops the LES methodology for compressible reacting flows. The configuration is described in section 5 and results are analysed in section 6.

2. Ignition of liquid rocket engines

The ignition of liquid rocket engines is a crucial phase. Due to high-speed injection jets and fast chemistry the ignition time is the key parameter for the success or failure of ignition : if it is too short, reactants are not sufficiently mixed to sustain combustion and if it is too long, the mixed reactants ignite strongly with high and dangerous pressure levels.

Figure 1 shows a simplified sketch of an injection plate supporting hundreds of coaxial injectors feeding a chamber connected to the exit nozzle. The ignition of the engine follows a specific sequence. First the system is purged with an inert gas (Helium) to reach a nominal state and to cool down injection lines. Then hydrogen injection starts and after a few milliseconds the igniter is triggered. In real engines, the igniter is either a pyrotechnic system or a spark torch (producing a strongly under-expanded jet in the chamber). Finally the oxidizer (O₂) is injected and combustion begins. Compared to combustion in conventional gas turbine for which LES was used before, ignition in rocket engines requires to take into account laser ignition, supersonic jets, H₂/O₂ chemistry and high speed flows. Trying to validate LES versus a laboratory experiment is the first objective of this paper.

3. The M3 burner experiment

The M3 burner experiment operated at DLR [12] has been designed to investigate ignition in a rocket like configuration, and more specifically the effect of injection conditions on ignition. Ignition is triggered thanks to a Nd:YAG ($\lambda = 532 \text{ nm}$) laser beam. Different injection regimes have been tested, resulting in multiple

ignition sequences [12]. The selected test case corresponds to a strong ignition (high maximum pressure), with a long intake phase that fills the chamber with a H₂-O₂ gaseous mixture before laser ignition. After ignition, the flame spreads over the whole chamber leading to a sharp pressure peak. Once the mixture is burnt, a diffusion flame anchors near the injector lips [12].

The test rig is fueled with gaseous hydrogen and oxygen by a coaxial injector and connected to the atmosphere by an exhaust nozzle (Fig. 2). The chamber is a 14 cm long box with a square section (6x6 cm²) designed to sustain pressures up to 20 bars (Fig. 2). Complete optical access to the chamber volume is obtained via two opposed quartz windows. On the two other sides smaller windows are used to introduce the igniting laser beam. Burnt gases exhaust through a 4 mm diameter nozzle. The coaxial injector is composed of a 1.22 mm diameter O₂ injection tube surrounded by a H₂ injection annulus with an inner diameter of 2 mm and an outer diameter of 4 mm (Fig. 2).

The laser ignites the mixture by an energy deposition of 195 mJ over 10 ns per pulse. The beam is focused in the mixing layer between the reactant jets, at 36 mm downstream the injection plate and at 2.5 mm above the injector axis (Fig. 2b). Schlieren images show that a hot plasma develops within an ellipsoid of 3.5 mm diameter and 2 mm length in the axial direction. No change of the flame behavior has been reported for energy depositions varying between 80 and 195 mJ.

Pressure and temperature probes are placed in the hydrogen and oxygen injection domes to measure their respective total pressures and temperatures (Fig. 2b), and pressure is also measured in the chamber. The data acquisition rate of these sensors is 4.35 kHz [12]. In addition Schlieren Photography (recorded thanks to a Hasselblag film camera with an aperture time of 13 μ s) is used to visualize the flow topology and the flame development. The Schlieren images show where density gradients are located (detecting the variation of refractive index into the gas). Density gradients appear in the jet where species segregation is present and between fresh and hot-burnt gases where the flame develops.

The experiment is operated at room temperature (≈ 300 K) and pressure (≈ 1.013 bar). Mass fluxes of hydrogen and oxygen are estimated thanks to choked nozzles located upstream of the domes in the injection lines, where pressures and temperatures are measured (Table 1).

In order to define a reference condition, the chamber and the injection lines are purged with N2 before each test (Table 2). Once nitrogen injection is stopped the propellants injection starts. Hydrogen and oxygen are injected at a mixture ratio of $\dot{m}_{O_2}/\dot{m}_{H_2} = 2$ corresponding to an equivalence ratio of 4. During the propellants injection phase, H2 is first injected alone for 7 ms, then the O2 valve is also opened. The injection phase lasts 370 ms before the laser is triggered.

4. LES of H2/O2 compressible reacting flows

4.1. Explicit compressible LES solver

A fully unstructured solver is used to advance the compressible Navier Stokes equations for a multi-species gas using perfect gas laws [15]. It is based on a finite volume formulation and an explicit integration scheme. Realistic thermochemistry is used, allowing multi-step kinetics for the oxidation of hydrogen [16]. For the present calculation, a one-step Runge-Kutta method is employed. Sub-grid scale turbulent viscosity is defined by the Smagorinsky model [17]. Characteristic boundary conditions are set with the NSCBC method [15, 18].

A summary of the LES equations solved by the code is given below [5] :

$$\frac{\partial \bar{\mathbf{w}}}{\partial t} + \nabla \cdot \bar{\mathbf{F}} = \bar{\mathbf{S}}_{\mathbf{c}} \quad (4.1)$$

where $\bar{\mathbf{w}}$ is the vector of conservative variables, $\bar{\mathbf{F}}$ is the flux tensor composed of viscous, inviscid and subgrid scale components and $\bar{\mathbf{S}}_{\mathbf{c}}$ is the chemical source term. $\bar{\mathbf{w}}$ and $\bar{\mathbf{S}}_{\mathbf{c}}$ are given respectively by :

$$\mathbf{w} = (\rho u, \rho v, \rho w, \rho E, \rho_k)^T \quad \text{and} \quad \bar{\mathbf{S}}_{\mathbf{c}} = (0, 0, 0, \omega_T + \dot{Q}, \omega_k)^T \quad (4.2)$$

where ρ is the density, $\mathbf{u} = (u, v, w)^T$ the velocity vector, the total energy per unit mass is defined by $E = \frac{1}{2} \mathbf{u} \cdot \mathbf{u} + E_i$ where E_i is the internal energy and $\rho_k = \rho Y_k$ where Y_k is the mass fraction of species k . The models for the reaction rates ω_k and the heat release ω_T in Eq. 4.2 are described in section 4.3. The \dot{Q} term is the power deposited by the laser (section 4.5).

4.2. Shock capturing in centered LES scheme

The conditions of injection in rocket engines lead to supersonic under-expanded jets with shocks in a succession of expansion/recompression cells [19]. This flow structure obviously has an impact on ignition

and must be reproduced. To capture shocks and slip lines present in the flow, the methodology of Cook and Cabot [20] is used to thicken the shock front by introducing a bulk viscosity β in the viscous stress tensor

$\underline{\tau}$:

$$\underline{\tau}_{modified} = \left(\beta - \frac{2}{3}\mu\right) \nabla \cdot \underline{\mathbf{u}} \underline{\delta} + 2\mu \underline{\underline{S}} \quad (4.3)$$

where μ is the dynamic viscosity and $\underline{\underline{S}}$ is the symmetric strain rate tensor. The bulk β viscosity is modeled as :

$$\beta = C(\Delta x)^4 |\nabla^2 \tilde{S}| \quad (4.4)$$

where C is fixed to 5. This bulk viscosity acts on the very sharp velocity gradients characterizing shocks but goes back to 0 where the velocity evolves smoothly. Tests have shown that it does not affect the LES quality away from shocks.

4.3. Chemical modeling for LES of H₂/O₂ combustion

A seven-step chemical scheme using six species (H₂, O₂, H₂O, OH, O, H) extracted from the work of Baurle [16] is used for the present LES (Table 3). This scheme accurately reproduces the laminar flame speed and adiabatic temperature over a large range of equivalence ratio and takes pressure effects into account. No tabulation is used and all species involved in the reactions of Table 3 are explicitly solved by the code. In the experiment the equivalence ratio (ϕ) of the H₂/O₂ mixture ranges from lean to very rich conditions ($\phi = 4$). Initially, the chamber pressure is equal to 1.85 bar and during ignition, the peak pressure reaches 11 bar.

Figure 3 shows the comparison between detailed chemistry [21] and the seven-step scheme for the prediction of the flame speed of premixed laminar flames. The laminar flame velocity is predicted with an error of about 10% around an equivalence ratio of 1.5 but is correct for both lean and rich conditions.

Figure 4 presents the laminar flame velocity plotted versus pressure (at $\phi = 1$) given by the seven-step scheme and compared to three detailed chemistries from Connaire [21], Kee [22] and Smooke [23]. Results show a maximum error of 18% at 10 bar between the seven-step scheme and the three detailed chemical schemes.

4.4. Flame turbulence interaction model

To handle flame/turbulence interaction, the dynamically thickened flame model (TFLES) is used [10, 24–27]. This model thickens the flame front by a factor F so that it can be resolved on the LES grid. The interaction between turbulence and chemistry is modelled through the so-called efficiency function, E [28] which accounts for the influence of the sub-grid scale wrinkling. The TFLES model has been applied successfully in several simulations (premixed and partially premixed) and more details can be found in Ref. [8, 10, 25, 28, 29].

4.5. Laser model for ignition in LES

A specific model (called ED for Energy Deposition) was built to describe the ignition by laser. This model simulates only the effect of the plasma on the surrounding gas and not the plasma itself (Fig. 5). In an electric or a laser spark, ignition does not occur within the plasma but in the unionized mixture around the hot kernel [30]. With the ED model, the plasma volume is neglected and the energy injected in the calculation domain is the energy transferred from the plasma to the gaseous mixture. For laser ignition this energy accounts for about 10% of the laser energy [31, 32] (most of the initial energy is lost in the created shock wave).

In the ED model, the laser is represented by a power \dot{Q} added to the energy equation 4.2. The \dot{Q} term is taken as a gaussian distribution in time and space deposited at the beam focus location :

$$\dot{Q}(x, y, z, t) = \frac{\varepsilon_i}{4\pi^2\sigma_r^3\sigma_t} e^{-\frac{1}{2}\left(\frac{r}{\sigma_r}\right)^2} e^{-\frac{1}{2}\left(\frac{t-t_o}{\sigma_t}\right)^2} \quad (4.5)$$

where r is the distance to the laser focus center, t_o is the time when \dot{Q} is maximum, ε_i is the total amount of deposited energy and σ_r and σ_t are the spatial and temporal widths of the deposition.

The energy deposition is focused at the same location as in the experiment. The shape of the kernel is simplified to a 6 mm diameter sphere, i.e. larger than the real diameter (3.5 mm), to allow a sufficient grid resolution. Similarly the pulse duration is increased to 500 ns (instead of 10 ns) to have a correct time resolution. Finally, the total amount of energy transferred to the mixture is set to 40 mJ, i.e. 20% of the Laser energy. Preliminary tests have shown that the size, duration and energy of the laser shot used in the LES had limited effect on the flame evolution because the laser shot is powerful enough to produce a successful ignition at every test even if the chemical run-away time varies.

5. Numerical configuration

The numerical configuration reproduces the 3D combustion chamber with the H2 dome, the O2 inlet tube and the exit throat (Fig. 6). The H2 dome is included in the computational domain to be able to capture the back-flow into the hydrogen injection line observed in the experiment. The oxygen injection is choked before ignition and becomes subsonic afterwards due to the chamber pressure rise. To minimize the impact of the exit boundary condition, the atmosphere around the chamber outlet is also calculated. The mesh is refined around the jets at inlet and downwards where the jets mix, develop and are ignited by the laser beam. It is fully unstructured and uses tetrahedral cells (Fig. 6c). It counts around 645,000 nodes, with the smallest and biggest cell characteristic size being of the order of 0.2 mm and 2 mm respectively.

5.1. Boundary conditions

A specific difficulty appears in such configurations, where the inlet velocity of a reactant (oxygen in the present case) is first sonic and then subsonic depending on the chamber pressure. To determine when the boundary condition must switch from sonic to subsonic, the momentum, temperature and pressure at inlet are calculated from the total pressure (P_i) in the dome and the chamber pressure (P_c), via isentropic nozzle relations between two reservoirs (with an appropriate discharge coefficient : C_d). Then the calculated velocity may be used to determine the flow regime and choose which variables to impose.

In the present case the oxygen inlet is first sonic as the oxygen dome is about 12 bars and the chamber is at atmospheric conditions, but after ignition, the chamber pressure increases up to 11 bars and the oxygen inlet goes to subsonic. The transition occurs when the chamber pressure P_c reaches the value $\left(\frac{2}{\gamma+1}\right)^{\frac{\gamma}{\gamma-1}} P_i$, where γ is the specific heat ratio, averaged on the injection surface.

For sonic and subsonic flows the mass flux is :

$$\dot{m} = AC_d \rho u_{inj} \quad (5.1)$$

where A is the throat section of the injector (Fig. 6b) and ρu_{inj} the inlet momentum.

In supersonic inlet conditions, all variables must be set and the inlet momentum is defined by [33] :

$$\rho u_{inj} = \frac{P_i}{\sqrt{r \cdot T_i}} \sqrt{\gamma} \left(\frac{2}{\gamma+1} \right)^{\frac{\gamma+1}{2(\gamma-1)}} \quad (5.2)$$

where T_i and P_i are respectively the total temperature and pressure in the dome. The static temperature

and pressure at injection are deduced from isentropic relations :

$$T_{inj} = \frac{2}{\gamma + 1} T_i \quad \text{and} \quad P_{inj} = \left(\frac{2}{\gamma + 1} \right)^{\frac{\gamma}{\gamma - 1}} P_i \quad (5.3)$$

Finally the density is calculated from the perfect gas equation of state.

In subsonic inlet conditions, only mass flux and temperature are imposed through a characteristic treatment (NSCBC) [15, 18]. They are calculated from isentropic relations now involving the chamber pressure P_c :

$$\rho u_{inj} = \frac{P_i}{\sqrt{r T_i}} \left(\frac{P_c}{P_i} \right)^{\frac{1}{\gamma}} \sqrt{\frac{2\gamma}{\gamma - 1} \left(1 - \left(\frac{P_c}{P_i} \right)^{\frac{\gamma - 1}{\gamma}} \right)} \quad (5.4)$$

$$T_{inj} = \left(1 + \frac{\gamma - 1}{2} M^2 \right)^{-1} T_i \quad (5.5)$$

where M is the Mach number at the injection surface.

The hydrogen inlet remains subsonic during the whole experiment. A characteristic treatment is used to set the subsonic mass flow rate and the static temperature (Tab. 1). These conditions are imposed at the H2 dome inlet (Fig. 6b).

The exit surface pressure (which is located outside the chamber, in the free atmosphere) is imposed to the ambient pressure using NSCBC [15, 18]. The walls in the injection lines and in the exhaust nozzle are adiabatic slip walls, whereas the chamber walls are treated with laws of the wall (for brevity this aspect has not been developed in this paper, more details are available in [34], [35]). The wall temperature is fixed at 300 K.

5.2. Initial conditions

The computation of the ignition sequence is performed in two steps. The first phase is the filling of the chamber with the gaseous reactants (H2 and O2). The chamber is initially full of nitrogen at 300 K and at a pressure of 1.013 bar. Then the ignition and the propagation of the flame are computed. Most of the filling phase (from 0 to 368 ms) is computed on a coarse mesh (390,000 nodes) and only the last instants (from 368 to 370 ms) are computed on the fine mesh (Fig. 6c) to establish the small scale structures and the mixture state prior ignition.

6. Results and discussion

6.1. The filling phase

At the ignition time the outlet nozzle is choked, the chamber pressure and temperature are respectively equal to 1.75 bar (6% lower than the experimental pressure) and 350 K. The instantaneous axial velocity field obtained by LES shows large recirculation zones around the jets with velocity magnitude of the order of 10 m/s. In the injection jet the velocity reaches a maximum value of 710 m/s corresponding to Mach 2.2. Figure 7a is a Schlieren image of the oxygen jet before ignition. A long succession of Mach cells can be noticed. This under-expanded jet is generated by the pressure ratio (equal to about 6) between the O₂ injection dome and the chamber. Figure 7b shows an instantaneous pressure field at $t=370$ ms (just before ignition), where several expansion/compression cells are observed, however the grid refinement in the simulation is not fine enough to capture all the Mach cells observed in the experiment. In the shear layer of the jet, high levels of turbulence are recorded and at the laser focus point the turbulence intensity of the axial velocity fluctuation is about 20%. Concerning chemistry and mixture properties, results show that some nitrogen remains in recirculation zone with a maximum of the mass fraction of 0.17. The reactants are well mixed in most of the chamber ($\phi = 4$). Segregation appears only in the injection jet : Fig. 7c shows a field of the mixture fraction at $t=370$ ms (just before ignition) and the local equivalence ratio is around 2 at the laser point.

6.2. Ignition and combustion

The solution obtained at the end of the intake phase at 370 ms is ignited by the laser model. After the energy deposition, the hot gas kernel is first convected downstream by the jet without being stretched. Then chemical reactions start and as the kernel grows its surface is increasingly wrinkled by turbulence. In this region $u'/S_l \approx 3$ (with u' the RMS of the velocity fluctuation and S_l the laminar flame speed).

Once the flame is initiated, it expands in all directions in the mixture of H₂-O₂. Five phenomena rule the flame propagation in the mixture : the expansion of the hot burnt gases, the convection due to the jet, the turbulence intensity, the local equivalence ratio of the mixture and its thermodynamics properties. Figure 8 shows series of snapshots of the fields of density gradient and velocity in the axial direction at three different times ($t = 30, 247, 681 \mu s$ after ignition). Schlieren photographs taken from experimental results at 35, 250 and 680 μs after ignition are also reported on Fig. 8. The flame front propagating towards the exit

is mainly driven by convective effects, the one developing towards the side walls is piloted by the dilatation of hot gases and the mixture conditions ($\phi = 4$). The flame front propagating towards the injection plate is composed of two different parts. One burns in the recirculation zone where the equivalent ratio is 4 following the same processes described earlier and the second one evolves into the jet (Fig. 8h). The latter is much more wrinkled by turbulence and encounters equivalence ratios near the stoichiometry. At $t = 681 \mu s$ after ignition, the flame burns the remaining mixture trapped near the walls. At this time, the hydrogen dome pressure is lower than the chamber pressure, the chamber mixture flows back into the injection dome and the flame is anchored to the injector (Fig 8i). This phenomenon is observed in the DLR experiment [12]. After complete combustion of the fuel trapped near the walls, the premixed flame extinguishes and only the flame stabilised at the injectors remains.

The corresponding pressure chamber evolution is presented in Fig. 9 and compared with experiment. The pressure increases sharply until the flame reaches the wall, then the increase slows down and the maximum is obtained when the last pocket of reactant mixture is consumed. Finally the pressure decreases due to the leakage by the nozzle.

7. Conclusions

A compressible LES methodology to compute flame ignition and propagation in a rocket engine fueled by oxygen and hydrogen has been derived and tested in the configuration of DLR [12]. This LES includes shocks computation, choked outlet and a six-species, seven-step chemical scheme for H₂/O₂ chemistry.

Results from LES are in good agreement with experimental observations, showing that the simulation captures the right mechanisms for flame ignition, propagation and stabilisation. The LES methodology for such compressible reacting flows, has been successfully used to reproduce violent delayed ignition in rocket engine conditions.

The methods exposed here are presently used to simulate an ignition transient in a simplified rocket engine fueled with liquid oxygen and gaseous hydrogen.

Acknowledgment

The authors gratefully acknowledge the support of Snecma DMS (Safran group) and of the computing center CINES, as well as DLR for fruitful discussions.

References

- [1] P. Moin, K. Squires, W. Cabot, S. Lee, *Phys. Fluids A* 3 (11) (1991) 2746–2757.
- [2] M. Lesieur, O. Métais, *Ann. Rev. Fluid Mech.* 28 (1996) 45 – 82.
- [3] M. Lesieur, in: O. Métais, J. Ferziger (Eds.), *New tools in turbulence modelling*, Les Editions de Physique - Springer Verlag, 1997, pp. 1 – 28.
- [4] H. Pitsch, *Ann. Rev. Fluid Mech.* 38 (2006) 453–482.
- [5] T. Poinsot, D. Veynante, *Theoretical and numerical combustion*, R.T. Edwards, 2nd edition., 2005.
- [6] J. Janicka, A. Sadiki, *Proc. of the Combustion Institute* 30 (2004) 537–547.
- [7] M. Freitag, J. Janicka, *Proc. of the Combustion Institute* 31 (2007) 1477–1485.
- [8] L. Selle, G. Lartigue, T. Poinsot, R. Koch, K.-U. Schildmacher, W. Krebs, B. Prade, P. Kaufmann, D. Veynante, *Combust. Flame* 137 (4) (2004) 489–505.
- [9] F. Di Mare, W. P. Jones, K. Menzies, *Combust. Flame* 137 (2001) 278–295.
- [10] P. Schmitt, T. Poinsot, B. Schuermans, K. Geigle, *J. Fluid Mech.* 570 (2007) 17–46.
- [11] A. Dauptain, *Allumage des moteurs fusée cryotechniques*, Ph.D. thesis, INPT - CERFACS (2006).
- [12] V. Schmidt, D. Klimenko, M. Oswald, *Preliminary results of test case "A" laser ignition tests for coaxial GH2/GO2-Injection*, Tech. rep., DLR, Lampoldshausen (2003).
- [13] V. Schmidt, D. Klimenko, O. Haidn, M. Oswald, A. Nicole, G. Ordonneau, M. Habiballah, *ONERA, TP no. 2004-49* 2004 (49).
- [14] S. Karl, K. Hannemann, in: *3rd International Workshop on Rocket Combustion Modeling*, 2006.
URL <http://elib.dlr.de/43913>
- [15] V. Moureau, G. Lartigue, Y. Sommerer, C. Angelberger, O. Colin, T. Poinsot, *J. Comput. Phys.* 202 (2) (2005) 710–736.
- [16] R. A. Baurle, S. Girimaji, *Combust. Flame* 134 (2003) 131–148.
- [17] J. Smagorinsky, *Month. Weath. Rev.* 91 (1963) 99–164.
- [18] T. Poinsot, S. Lele, *J. Comput. Phys.* 101 (1) (1992) 104–129.
- [19] P. Thompson, *Compressible-fluid dynamics*, McGraw-Hill, 1972.
- [20] A. W. Cook, W. H. Cabot, *J. Comput. Phys.* 203 (2005) 379–385.

- [21] M. Connaire, H. Curran, J. Simmie, W. Pitz, C. Westbrook, *International Journal of Chemical Kinetics* 36 (11) (2004) 603–622.
- [22] R. Kee, J. Warnatz, J. Miller, *A fortran computer code package for the evaluation of gas phase viscosities, conductivities, and diffusion coefficients*, Tech. Rep. SAND83-8209, Sandia National Laboratories (1983).
- [23] M. Smooke, M. Koszykowski, *Fully adaptive solutions of one-dimensional mixed initial-boundary value problem with applications to unstable problems in combustion*, Tech. Rep. SAND 83-8219, Sandia National Laboratories (1983).
- [24] J.-P. L egier, T. Poinso, D. Veynante, in: *Summer Program 2000*, Center for Turbulence Research, Stanford, USA, 2000, pp. 157–168.
- [25] C. Martin, L. Benoit, Y. Sommerer, F. Nicoud, T. Poinso, *AIAA Journal* 44 (4) (2006) 741–750.
- [26] A. Sengissen, A. Giauque, G. Staffelbach, M. Porta, W. Krebs, P. Kaufmann, T. Poinso, *Proc. of the Combustion Institute* 31 (2007) 1729–1736.
- [27] G. Staffelbach, *Simulation aux grandes  echelles des instabilit es de combustion dans les configurations multi-br uleurs*, Ph.D. thesis, Institut National Polytechnique de Toulouse (2006).
- [28] O. Colin, F. Ducros, D. Veynante, T. Poinso, *Phys. Fluids* 12 (7) (2000) 1843–1863.
- [29] C. Angelberger, F. Egolfopoulos, D. Veynante, *Flow Turb. and Combustion* 65 (2) (2000) 205–22.
- [30] T. Spiglanin, A. Mcilroy, E. Fournier, R. Cohen, J. Syage, *Combust. Flame* 102 (3) (1995) 310–328.
- [31] D. Bradley, C. Sheppard, I. Suardjaja, R. Woolley, *Combust. Flame* 138 (2004) 55–77.
- [32] T. Phuoc, F. White, *Proc. of the Combustion Institute* 29 (2002) 1621 – 1628.
- [33] A. H. Shapiro, *The Dynamics and Thermodynamics of Compressible Fluid Flow*, Wiley, 1953.
- [34] P. Schmitt, *Simulation aux grandes  echelles de la combustion  etag ee dans les turbines  a gaz et son interaction stabilit e-polluants-thermique*, Ph.D. thesis, INP Toulouse (2005).
- [35] D. Panara, M. Porta, R. Dannecker, B. Noll, in: *Proceedings of the 5th International Symposium on Turbulence, Heat and Mass Transfer.*, 2006.

8. Tables

cold flow	O2	1.135
mass fluxes [g/s]	H2	0.592
Dome total	O2	300
temperatures [K]	H2	302
Dome total	O2	11.7
Pressures [bar]	H2	2.1
Pressure of the chamber [bar]		1.87

Table 1: Injection conditions for the M3 test case (at ignition time).

N2 valve closure : t_{N2}	-1000ms
H2 valve opening : t_{H2}	0 ms
O2 valve opening : t_{O2}	7 ms
laser ignition : $t_{ignition}$	370 ms

Table 2: Time sequence for the M3 test case.

Reaction	A	β	Ea
$H + O_2 = O + OH$	3.62E+17	-0.91	1.653E+4
$O + H_2 = H + OH$	1.53E+5	2.67	6.296E+3
$O_2 + H_2 = OH + OH$	5.13E+13	0.00	4.805E+4
$OH + H_2 = H_2O + H$	6.64E+13	0.00	5.155E+3
$OH + OH = H_2O + O$	1.90E+13	0.00	1.091E+3
$H + OH + M =$	6.67E+22	-2.00	0.000
$H_2O + M$			
$H + H + M = H_2 + M$	2.20E+18	-1.00	0.000
third body efficiencies :			
2.5 for H_2 , 16 for H_2O and 1.0 for all other M			
A : [cm³/mole.sec] ; Ea : [cal/mole]			

Table 3: The seven-step H2-O2 kinetic scheme.

9. Figures

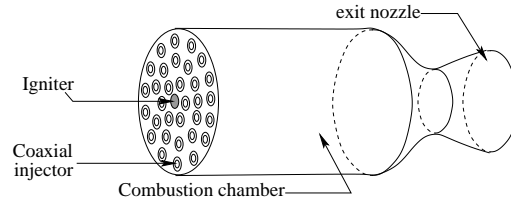


Fig. 1: Sketch of a real combustion chamber.

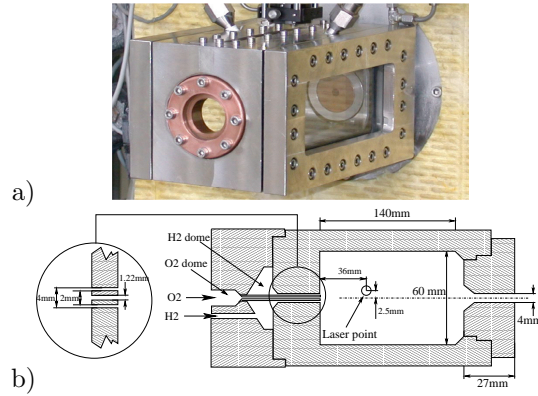


Fig. 2: The Micro-Combustor M3. a) Photograph. b) Geometry.

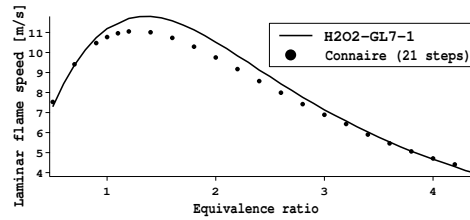


Fig. 3: Chemical comparison of the laminar flame speed given by the seven-step scheme (H2O2-GL7-1) used for the computation and a detailed chemistry from Connaire [21] ($T_{cold\ gas} = 300K$ $P=2.0\ bar$).

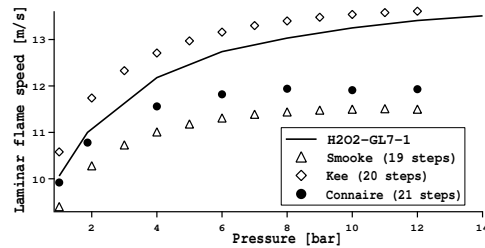


Fig. 4: Laminar flame speed against pressure, comparison between the seven-step scheme (H2O2-GL7-1) and three detailed chemistries from Connaire [21], Smooke [23] and Kee [22] ($T_{cold\ gas} = 300K$, $\phi = 1.0$).

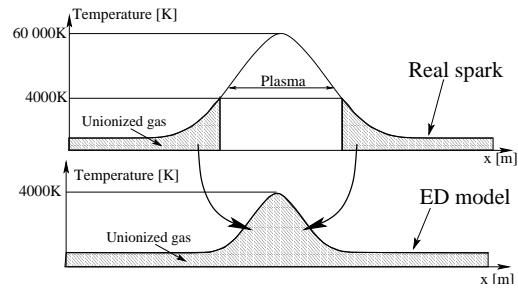


Fig. 5: Sketch of the temperature profile inside a spark kernel and part of the flow modeled with the ED model. With the ED model, only the effect of the plasma on the surrounding unionized gas is simulated.

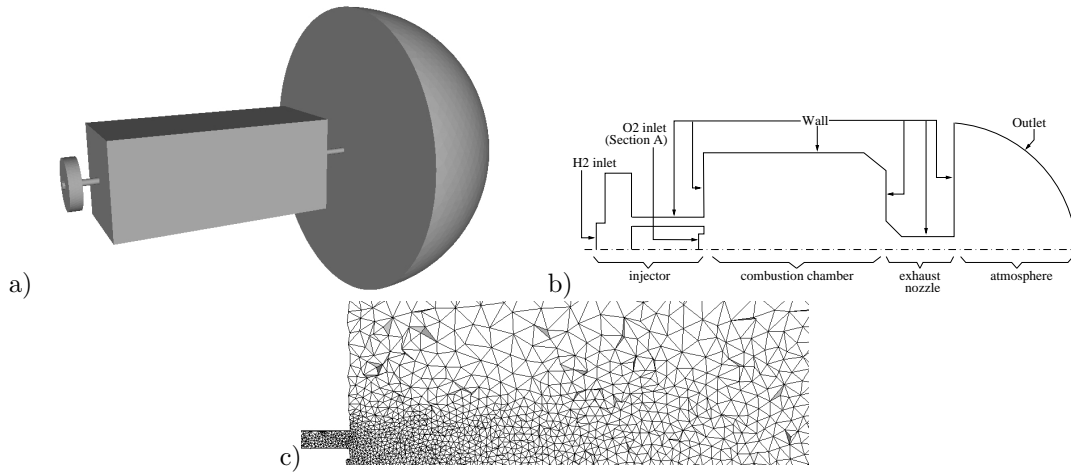


Fig. 6: Computing domain for the M3 Micro-combustor. a) Geometry b) Sketch of boundary conditions c) Zoom around the inlet region.

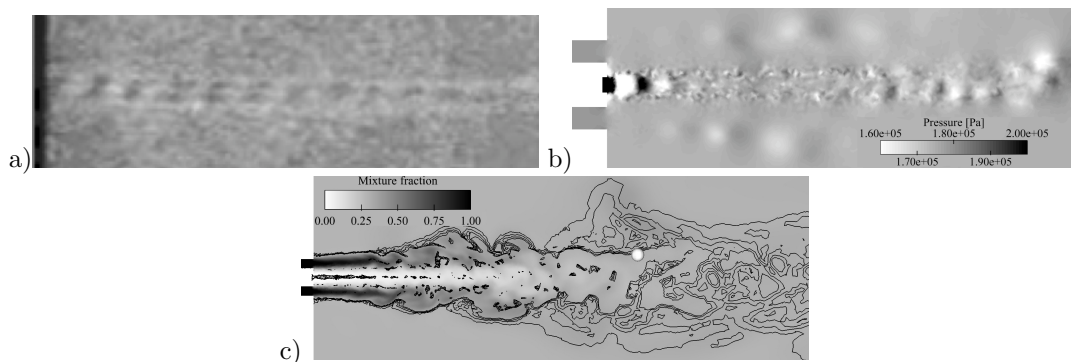


Fig. 7: Flow conditions at the injector outlet before ignition. a) Schlieren picture of the oxygen jet, b) pressure field, c) mixture fraction field, black iso-lines : vorticity and white point : laser location.

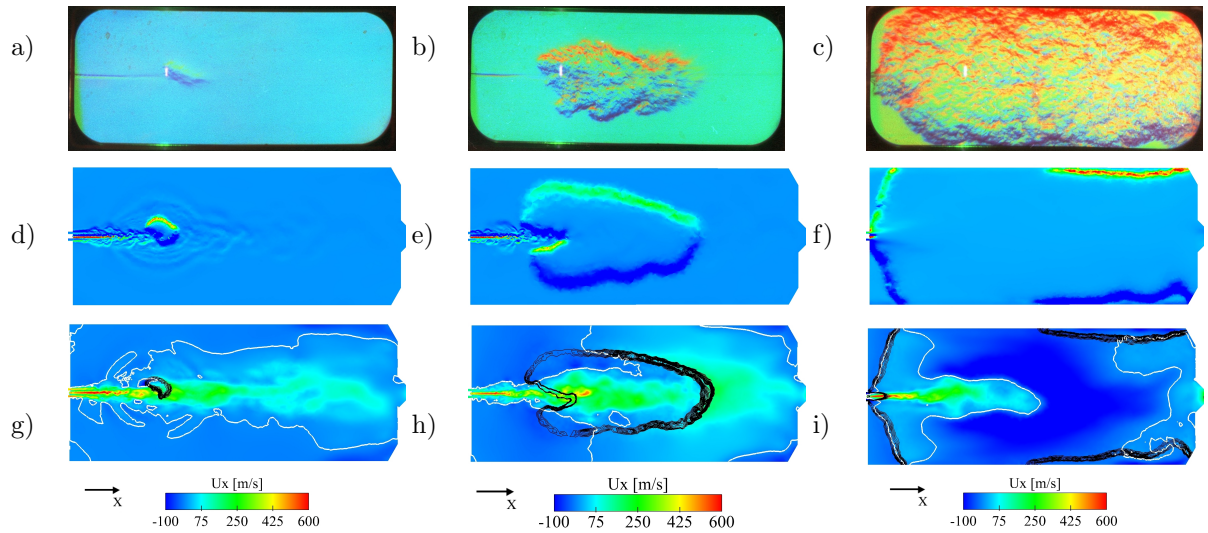


Fig. 8: Schlieren photographs (experiment) at three different times after ignition (a) $t = 35\mu s$, b) $t = 250\mu s$, c) $t = 680\mu s$), snapshots of the density gradient field (LES results) at three different times after ignition (d) $t = 30\mu s$, e) $t = 247\mu s$, f) $t = 681\mu s$) and snapshots of the axial velocity with a $U_x = 0$ m/s isoline (white) and reaction-rate isolines (black) at three different times after ignition (g) $t = 30\mu s$, h) $t = 247\mu s$, i) $t = 681\mu s$).

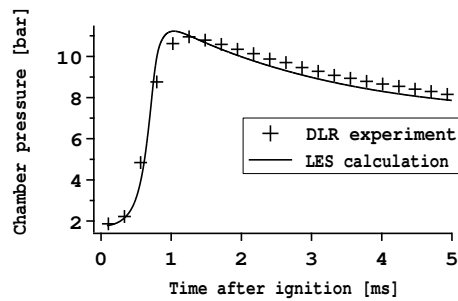


Fig. 9: Temporal evolution of the mean chamber pressure compared with experiment.